Published in final edited form as:

Sci Transl Med. 2016 August 10; 8(351): 351ra107. doi:10.1126/scitranslmed.aaf7837.

Loss-of-function mutations in the RNA biogenesis factor *NAF1* predispose to pulmonary fibrosis–emphysema

Susan E. Stanley[1,2,*], **Dustin L. Gable**[1,2,*], **Christa L. Wagner**[1], **Thomas M. Carlile**[3], **Vidya Sagar Hanumanthu**[1], **Joshua D. Podlevsky**[4], **Sara E. Khalil**[1], **Amy E. DeZern**[1,5,6], **Maria F. Rojas-Duran**[3], **Carolyn D. Applegate**[1,6,7], **Jonathan K. Alder**[1], **Erin M. Parry**[1,5], **Wendy V. Gilbert**[3], and **Mary Armanios**[1,6,7,†]

[1]Department of Oncology, Johns Hopkins University School of Medicine, Baltimore, MD 21287, USA.

[2]Medical Scientist Training Program, Johns Hopkins University School of Medicine, Baltimore, MD 21287, USA.

[3]Department of Biology, Massachusetts Institute of Technology, Cambridge, MA 02139, USA.

[4]Department of Chemistry and Biochemistry, Arizona State University, Tempe, AZ 85277, USA.

[5]Department of Medicine, Johns Hopkins University School of Medicine, Baltimore, MD 21287, USA.

[6]Sidney Kimmel Comprehensive Cancer Center, Johns Hopkins University School of Medicine, Baltimore, MD 21287, USA.

[7]McKusick-Nathans Institute of Genetic Medicine, Johns Hopkins University School of Medicine, Baltimore, MD 21287, USA.

[†]Corresponding author. marmani1@jhmi.edu.
[*]These authors contributed equally to this work.

SUPPLEMENTARY MATERIALS

www.sciencetranslationalmedicine.org/cgi/content/full/8/351/351ra107/DC1

Materials and Methods

Fig. S1. Characteristics of PF-emphysema probands cases studied.

Fig. S2. Detailed clinical history of short telomere syndrome features in *NAF1* mutation carriers.

Fig. S3. Full-length NAF1 cDNA rescues TR levels in homozygous mutant HCT116 cells.

Fig. S4. Multispecies NAF1 alignment showing conserved motifs.

Fig. S5. Leptomycin B blocks nuclear export and TR levels after nuclear localization is restored for $NAF1^{K319fs}$.

Fig. S6. Schema of mouse box H/ACA snoRNAs quantified showing the complementary guide sequence and the rRNA Ψ target site.

Table S1. Mouse rRNA Ψ sites mapped on the basis of homology and analyzed by Pseudo-seq ($n = 107$).

References (*62*–*72*)

Author contributions: S.E.S. and M.A. conceived the idea, evaluated the index family, and designed the screen. S.E.S. performed the genome sequencing and designed and performed the human studies. S.E.S. and D.L.G. designed and performed the CRISPR/Cas9 experiments. D.L.G. and M.A. designed the mouse experiments, and D.L.G. performed them. C.L.W. performed cell culture experiments with S.E.S. and D.L.G. T.M.C. and M.F.R.-D. prepared the Pseudo-seq libraries, and T.M.C. analyzed the data and interpreted them with W.V.G. V.S.H. performed the telomere length measurements and Northern blotting with input from C.L.W. J.D.P. performed the multispecies alignment. C.D.A., A.E.D., and E.M.P. assessed clinical data. S.E.K. performed the fractionation and immunofluorescence quantification. J.K.A. and E.M.P. performed and analyzed some of the genomic data. S.E.S. and M.A. wrote the manuscript with input from D.L.G. All the authors reviewed and gave comments on the manuscript.

Competing interests: The authors declare that they have no competing interests.

Data and materials availability: The data for this study have been deposited in the National Center for Biotechnology Information Gene Expression Omnibus database (submission ID 17772667, accession ID GSE78063).

Abstract

Chronic obstructive pulmonary disease and pulmonary fibrosis have been hypothesized to represent premature aging phenotypes. At times, they cluster in families, but the genetic basis is not understood. We identified rare, frameshift mutations in the gene for nuclear assembly factor 1, *NAF1*, a box H/ACA RNA biogenesis factor, in pulmonary fibrosis–emphysema patients. The mutations segregated with short telomere length, low telomerase RNA levels, and extrapulmonary manifestations including myelodysplastic syndrome and liver disease. A truncated NAF1 was detected in cells derived from patients, and, in cells in which the frameshift mutation was introduced by genome editing, telomerase RNA levels were reduced. The mutant NAF1 lacked a conserved carboxyl-terminal motif, which we show is required for nuclear localization. To understand the disease mechanism, we used CRISPR (clustered regularly interspaced short palindromic repeats)/Cas9 (CRISPR-associated protein-9 nuclease) to generate *Naf1*$^{+/-}$ mice and found that they had half the levels of telomerase RNA. Other box H/ACA RNA levels were also decreased, but rRNA pseudouridylation, which is guided by snoRNAs, was intact. Moreover, first-generation *Naf1*$^{+/-}$ mice showed no evidence of ribosomal pathology. Our data indicate that disease in *NAF1* mutation carriers is telomere-mediated; they show that NAF1 haploinsufficiency selectively disturbs telomere length homeostasis by decreasing the levels of telomerase RNA while sparing rRNA pseudouridylation.

Tidy telomeres make for healthier lungs

Telomeres are the protective caps that prevent the ends of chromosomes from unraveling. People carrying mutations in the protein or RNA component of telomerase, the enzyme that makes telomeres have short telomeres and a serious and often fatal lung disease– –pulmonary fibrosis. Now, Stanley *et al.* find in several patients that other mutations, specifically those that interfere with RNA biogenesis, can also cause both short telomeres and lung disease. This work expands our understanding of how telomeres are maintained and their role in human disease.

INTRODUCTION

Lung disease is the third leading cause of death in the United States (1). Chronic obstructive pulmonary disease (COPD), which includes emphysema, and pulmonary fibrosis (PF) are major culprits. Both diseases have been shown to cocluster at times in families that show autosomal dominant inheritance; however, the genetic basis in most of these cases is not understood (2–5). A number of observations have linked the etiology of PF and emphysema to premature aging and to abnormalities in telomere length maintenance (3, 6–10). For example, abnormally short telomere length is a frequent finding in at least half of idiopathic PF patients (6, 11). Moreover, clinical features of a short telomere syndrome, including bone marrow failure/myelodysplastic syndrome, liver disease, and infertility, are common in patients with sporadic and familial PF, as well as in some patients with emphysema (6, 12–15). The diagnosis of a short telomere syndrome in these patients is relevant for patient care because the defect is systemic, and they show exquisite sensitivity to otherwise tolerated medications and procedures, especially in the setting of lung transplantation (16). Mutations in the core telomerase enzyme components—*TERT*, the reverse transcriptase, and *TR*, the telomerase RNA component—were the first to be linked to inherited forms of PF; they are

the most common identifiable genetic abnormality, and collectively they explain 15 to 20% of familial PF cases (2, 17–19). Smokers with telomerase mutations, especially women, are also prone to developing emphysema, alone or combined with PF (3). In smokers with severe, early-onset emphysema, *TERT* mutations were recently reported to be a risk factor in a proportion comparable to that of α-1 antitrypsin deficiency (3). However, in 70% of families with autosomal dominant PF, the genetic basis remains uncharacterized (2), and, aside from *TERT*, the other heretofore identified telomere genes—*TR, DKC1, TINF2, RTEL1*, and *PARN*—each explains only 1 to 3%of familial cases (13, 15, 20, 21).

Vertebrate TR shares with a family of noncoding RNAs a 3′ box H/ACA motif; this domain is required for its stability and assembly into a mature telomerase holoenzyme complex (22–24). To overcome the challenge caused by the locus heterogeneity in familial PF-emphysema, we classified genetically uncharacterized cases by molecular abnormality using TR levels as a stratification tool and examined candidate genes that have been implicated in TR biogenesis.

RESULTS

Rare variants in *NAF1* segregate with short telomere phenotype and low TR levels

To probe the genetic basis of uncharacterized familial PF-emphysema, we performed whole-genome sequencing on five unrelated probands who had abnormally short telomeres, extrapulmonary telomere syndrome features, and a family history consistent with autosomal dominant inheritance (fig. S1, A to C), but found no shared rare variants. To narrow the candidates, we subclassified the cases by TR levels in lymphoblastoid cell lines (LCLs). Three probands had half the TR levels of controls as measured by quantitative reverse transcription real-time polymerase chain reaction (qRT-PCR) (fig. S1D), and we selected these for a candidate search that prioritized TR biogenesis genes. We included pontin (*RUVBL1*) and reptin (*RUVBL2*), adenosine triphosphatases that facilitate telomerase assembly (25), as well as *GAR1, SHQ1*, and *NAF1* (nuclear assembly factor 1), which are involved in TR biogenesis (26–31). In JH1, a proband with combined PF and emphysema, we found a heterozygous single base pair (bp) insertion in exon 7 of *NAF1*, c.984insA, which predicted a premature stop after a short, out-of-frame amino acid sequence, S329Ifs*12(Fig. 1, A and B). This variant had not been seen in 9006 individuals reported in public databases and was absent in 134 controls that we also sequenced (Fig. 1C). S329Ifs*12 was present in the proband's two siblings who had short telomere disease phenotypes, as well as in her mother who died from emphysema, but was absent in unaffected relatives (Fig. 1A and fig. S2). An affected sibling similarly had low TR levels relative to controls (Fig. 1D), as well as abnormally short telomeres, whereas noncarriers in the family had longer telomeres (Fig. 1, E and F), albeit the telomeres were not as long in the proband's son, consistent with the known inheritance of short telomeres in offspring of telomerase mutation carriers (32–34).

To examine the prevalence of mutations, we sequenced*NAF1* in 25 additional genetically uncharacterized cases with PF, alone or combined with emphysema. Among them, we identified JH2, a woman with sporadic idiopathic PF and bone marrow failure, who carried a heterozygous 2-bp deletion, also in exon 7, c.956_957delAA, which predicted a frameshift

followed by a premature stop, K319Rfs*21 (Fig. 1, A and B). This second variant was also absent from the public databases and from the controls that we sequenced (Fig. 1C). Leukocyte telomere length was abnormally short in this patient (Fig. 1, E and F), and her peripheral blood cells failed several transformations with Epstein-Barr virus, presumably because of the severity of the telomere defect. Altogether, rare *NAF1* variants were detected in 2 of 30 (7%) genetically uncharacterized PF-emphysema patients in our cohort.

A truncated NAF1 protein in mutation carriers

We examined the consequences of the frameshifts that we identified on protein stability. NAF1 is a 494–amino acid protein, and if the truncated proteins were stable, a 339– and 338–amino acid product would be seen in JH1 and JH2, respectively (Fig. 2A). Protein lysates from patient-derived LCLs from JH1 and her sibling showed that there was nearly half the level of full-length NAF1 compared to unrelated controls and to the relative who did not carry the mutation. A lower–molecularweight species that was only seen in mutation carriers was also detected; it corresponded to the predicted weight of the truncated protein (Fig. 2B). To determine whether the frameshift mutations could give rise to a shortened species, we expressed N-terminal Myc-tagged K319Rfs*21 and S329Ifs*12 (hereon K319fs and S329fs, respectively) under the control of a doxycycline-inducible cytomegalovirus promoter at an isogenic locus in HeLa cells. In this system, we detected shortened NAF1 proteins that migrated at a molecular weight similar to the truncated species that we observed in patient-derived cells and to the predicted product for K319fs, respectively (Fig. 2C). When overexpressed, these mutants did not compromise TR levels (85 and 100% of control levels for K319fs and S329fs, respectively; $P = 0.7$ for both), indicating that they did not exert a dominant-negative effect. In contrast, short hairpin RNA (shRNA) knockdown of the endogenousNAF1 decreased TR levels (Fig. 2, D to F). The decrease in overall TR was independent of dyskerin because its levels were intact in LCLs from mutation carriers (Fig. 2B). These data suggested that NAF1 loss of function likely underlies the telomerase insufficiency in the patients that we identified.

Disease-associated *NAF1* alleles are functionally deleterious

To directly test the pathogenicity of the rare alleles, we compared their capacity to rescue TR levels after NAF1 knockdown in HeLa cells (Fig. 2G). K319fs failed to rescue TR, but S329fs was comparable to the wild-type allele in this system, suggesting that it had residual function when overexpressed (Fig. 2H). To test the consequences of the S329fs allele on TR stability at its endogenous levels, we used CRISPR (clustered regularly interspaced short palindromic repeats)/Cas9 (CRISPR-associated 9) to knock in the mutation in pseudodiploid HCT116 cells. A homozygous mutant clone, $NAF1^{S329fs/S329fs}$, was derived, and it expressed only the truncated NAF1 species (Fig. 2, I and J). This clone exhibited significantly decreased TR levels (31 and 14% of control cells by qRT-PCR and Northern blot, respectively; Fig. 2, K to I). Restoring full-length NAF1 by lentiviral complementary DNA (cDNA) transduction partially rescued TR, consistent with a NAF1-dependent effect on telomerase levels in these cells (fig. S3, A to C).

NAF1 mutations impair nuclear localization

To understand how the mutant NAF1 proteins compromised TR, we examined the conserved domains within the truncated regions. K319fs and S329fs fell near a bipartite, lysine-rich NLS that is functionally conserved in yeast (Fig. 3A and fig. S4) (31, 35, 36). K319fs disrupted the entire NLS, but S329fs interrupted only half the sequence (Fig. 3A). Additionally, K319fs interrupted a highly conserved portion of the Gar1 homology domain (Fig. 3A and fig. S4). To test whether the truncated NAF1 proteins were defective for nuclear localization, we tracked the nuclear fraction of Myc-tagged proteins by immunofluorescence in the modified HeLa cells after treatment with leptomycin B, a blocker of nuclear export. Leptomycin B abolished the export of $NAF1^{WT}$, and it accumulated in the nucleus, as expected (fig. S5A). In contrast, when four lysines, previously linked to nuclear localization (36), were mutated to alanine ($NAF1^{4K>4A}$), there was a greater fraction in the cytoplasm (Fig. 3, A to D). Similar to$NAF1^{4K>4A}$, $NAF1^{K319fs}$ and$NAF1^{S329fs}$ were both enriched in the cytoplasm (Fig. 3, C and D). The nuclear localization defect was more pronounced for $NAF1^{K319fs}$, consistent with our earlier results showing that $NAF1^{S329fs}$ is hypomorphic (Fig. 3, C and D; also see Fig. 2H). We also tested whether a nuclear localization defect was present in $NAF1^{S329fs/S329fs}$ HCT116 cells and documented a decreased NAF1 nuclear fraction by Western blot (mean, 44% of controls; n = 5 experiments; range, 33 to 69%; P = 0.002; representative gel in Fig. 3E). To assess the functional relevance of these observations, we probed whether an exogenous NLS can rescue the localization. We added an exogenous SV40-derived NLS sequence onto the N terminus of each of the mutant proteins and found that the nuclear localization was restored (Fig. 3, A to D). However, for $NAF1^{K319}$, the exogenous NLS could not rescue TR levels after shRNA knockdown, suggesting that the Gar1 homology domain altered in this mutant protein is also required for TR stability (fig. S5, B and C).

Naf1 is an essential gene

Because NAF1 has been implicated in the biogenesis of H/ACA RNAs beyond TR (27), we sought to understand the molecular mechanism underlying the disease phenotype in *NAF1* mutation carriers. We used CRISPR/Cas9 to disrupt the *Naf1* gene in mice and identified a founder with a heterozygous 322-bp deletion in exon 1 that predicted a null allele (Fig. 4A); this mouse had half theNAF1 levels by Western blot (Fig. 4, B and C). Interbreeding these $Naf1^{+/-}$ mice yielded no homozygous null pups (>200 screened; P < 0.001, Fisher's exact test), and there were no null embryos detected between E8.5 and E12.5 (n = 32 screened; P < 0.01). Because the $TR^{-/-}$ mouse is viable (37), these data were consistent with NAF1 having essential roles in RNA biogenesis beyond TR.

$Naf1^{+/-}$ mice have half the levels of TR, but ribosomal RNA pseudouridylation is preserved

We next tested the consequences of *Naf1* heterozygosity on H/ACA RNA stability. As with the human mutation carriers, we found that TR levels in $Naf1^{+/-}$ mice were decreased, similar to $TR^{+/-}$ animals (61 and 44% of controls, by qRT-PCR and Northern blot, respectively; Fig. 4, D and E). Moreover, the levels of H/ACA small nucleolar RNAs (snoRNAs) and a small Cajal body RNA were also reduced (mean, 63%; range, 46 to 74%; Fig. 4F; P < 0.05 for three of the seven RNAs assayed). Because H/ACA snoRNAs guide

ribosomal RNA (rRNA) pseudouridylation (38), we examined whether their decreased levels affected their target rRNA site modification. We identified 107 pseudouridines (Ψs) by homology to human rRNA sites (table S1) and comprehensively quantified their pseudouridylation with the recently developed Pseudo-seq method (39). The aggregate Ψ signal across all the Ψs detected in *Naf1*$^{+/-}$ mice was not significantly different from wild type (96.7%; $P = 0.2$, unpaired t test; Fig. 4G). Examining each individual rRNA site revealed a similar Pseudo-seq signal in *Naf1*$^{+/-}$ mice, well within the intragroup variability of this high-resolution technique (mean *Naf1*$^{+/-}$:*Naf1*$^{+/+}$ ratio, 0.95; Fig. 4, H and I). To determine whether there were physiologic consequences resulting from the decreased H/ACA RNA levels, we examined first-generation *Naf1*$^{+/-}$ mice for survival and skeletal defects, weight loss, and cytopenias but found no evidence of pathology. Specifically, and in contrast to mice with loss of function of ribosome genes (40), *Naf1*$^{+/-}$ mice had no abnormalities in hematopoiesis and had intact function and histology of all their major organs.

DISCUSSION

We report here that *NAF1* loss-of-function mutations cause a short telomere syndrome that manifests as PF-emphysema, as well as extrapulmonary telomere-mediated disease. Although mutations in the core telomerase components, *TERT* and *TR*, cause haploinsufficiency and autosomal dominant disease (17, 33, 41, 42), mutations in other, previously identified telomerase biogenesis factors have shown recessive inheritance (43–45). NAF1 may thus beunique among the RNA biogenesis factors in that it is required at full dosage for telomerase and telomere maintenance. Supporting this observation, a single-nucleotide polymorphism (SNP) near the *NAF1* locus is the only variant near a telomerase-related gene to be identified in genome-wide association studies for telomere length, aside from *TERT* and *TR* (46, 47). rs7675998, which falls 40 kb downstream of *NAF1*, has an effect size on telomere length similar to SNPs near *TERT* and *TR* (46, 47). Our data suggest that this SNP affects telomere length by compromising NAF1 levels. rs7675998 has also been reported to be protective against melanoma (48), likely also by promoting telomere shortening, which lowers melanoma risk (2). The exquisite sensitivity of telomere length maintenance to NAF1 levels that we identified here in Mendelian short telomere syndromes thus sheds light on the molecular basis of disorders with complex inheritance.

NAF1 functions to stabilize H/ACA RNAs, a family that includes more than 100 members. Among them, snoRNAs are most common (49). Although we found that *Naf1*$^{+/-}$ mice had decreased H/ACA RNA levels, their targeting of rRNA modification was spared. In contrast, haploinsufficiency for TR causes telomere shortening in late-generation *TR*$^{+/-}$ mice (33, 50). The intact phenotype of first-generation *Naf1*$^{+/-}$ mice, despite the decreased H/ACA RNA levels, suggests that they behave similarly to early-generation *TR*$^{+/-}$ mice. However, in stark contrast to *TR*$^{-/-}$ mice, which are viable, we found that mammalian *NAF1* is essential, likely because of its conserved role in rRNA modification, as had been observed in yeast (30, 51, 52). Despite the decrease in H/ACA snoRNA levels, we found that ribosome pseudouridylation in *Naf1*$^{+/-}$ mice was intact. The basis underlying the selective sensitivity to heterozygous loss of *NAF1* in telomere length maintenance may be explained by the low abundance of TR relative to other H/ACA RNAs (for example, snoRNAs having 50-fold or

higher levels). Factors other than absolute RNA levels may also play a role. For example, TR may be specifically vulnerable to NAF1 loss because, in contrast to other box H/ACAs, it has its own transcriptional regulation and is not protected by an intron lariat (53). Because the natural histories of the patients that we studied were indistinguishable from those of *TR* mutation carriers and because early-generation *Naf1*$^{+/-}$ mice have no evident pathology, our data support the conclusion that *NAF1* hapoloinsufficiency causes disease in a manner dependent on telomerase.

The role of telomerase and telomere shortening in mediating lung disease has been studied in animal models. Although telomerase insufficiency alone does not cause lung pathology, telomerase-null mice with short telomeres develop emphysema when exposed to cigarette smoke (8). The pathology has been linked to cumulative injury in epithelial cells that is caused by additive genotoxic damage from cigarette smoke superimposed on telomere dyfunction. When telomere dysfunction is induced in alveolar stem cells, they show hallmarks of senescence, and the lungs show remodeling that manifests as an emphysema-like phenotype associated with recruitment of an inflammatory response resembling that seen in COPD (9). Our findings here, in the context of the published literature, highlight how telomere shortening is a relevant mechanism for PF-emphysema susceptibility in a subset of patients beyond those with mutations in the telomerase core components. It is thus possible that efforts to reverse the telomere defect, or other regenerative approaches, will influence the natural history of these progressive pathologies in patients with telomere-mediated lung disease.

MATERIALS AND METHODS

Study design

The goal of this study was to discover novel genes that cause familial short telomere syndromes. Probands with IPF-emphysema with pedigrees that show autosomal dominant inheritance were stratified by TR levels, and genomic DNA was analyzed by whole-genome sequencing and candidate gene examination. To test whether the identified variants caused disease, their segregation with the short telomere phenotype and TR levels were examined, and their frequency in healthy controls was queried. To understand the functional consequences of mutations, a multispecies alignment was generated. The cellular and molecular consequences of the mutations were studied in patient-derived LCLs, as well as in an inducible HeLa system where mutants were knocked in at an isogenic locus. CRISPR/Cas9 editing was used to introduce the mutations at the endogenous locus and study the effect on TR stability. To model *NAF1* loss of function at the organismal level, the *Naf1* gene was disrupted in single-cell mouse zygotes with CRISPR/Cas9, and the clinical phenotype was examined in blinded studies. To test the consequences of *Naf1* loss on ribosome modification, we mapped mouse rRNA sites and performed Pseudo-seq to quantify the pseudouridylation signal. All the immunofluorescence, Northern blotting, and Pseudo-seq studies were performed blinded to genotype. All the studies were performed at a minimum of triplicate. Other details regarding the replication of the data are included in the respective figure legends.

Subjects

Subjects were recruited from 2007 to 2015 as part of the Johns Hopkins Telomere Syndrome Registry. Entry criteria included familial PF-emphysema or familial/sporadic cases with classic short telomere syndrome phenotypes and molecularly documented short telomere length as described (12, 54, 55). Control DNA (n = 134) was obtained from the National Disease Research Interchange from individuals who had no lung disease, and the donors self-identified as being of European ancestry. Peripheral blood mononuclear cells were transformed with Epstein-Barr virus as described (56). Among the 25 genetically uncharacterized cases that were screened, 16 had familial PF, and 9 had sporadic PF-emphysema with extrapulmonary telomere syndrome features. The study was approved by the Johns Hopkins Medicine Institutional Review Board, and all the subjects gave written, informed consent.

Telomere length measurement

Telomere length was measured by flow-FISH (57) in a Johns Hopkins Clinical Laboratory Improvement Amendment–certified facility. The flow-FISH method includes extensive controls, including MESF (molecules of equivalent soluble fluorochrome) beads, cow thymocyte internal control, and standards on each plate prepared as described (57). The facility's intra-assay coefficient of variation (CV) among the three replicate samples had a mean of 1.2 and 0.8%, and the inter-assay CV was 1.8 and 0.7% for lymphocytes and granulocytes, respectively. Telomere data were plotted relative to a validated nomogram derived from healthy controls (13, 18).

DNA extraction, next-generation sequencing, and variant filtering

Genomic DNA from peripheral blood was isolated using the PureGene Blood Core Kit (Qiagen). For whole-genome sequencing, genomic DNA libraries were prepared without amplification with the TruSeq DNA PCR-Free sample preparation kit (Illumina). Short-read, paired-end sequencing was carried out with the Illumina HiSeq 2000 platform. Reads were aligned to the GRCh37 reference genome with the Illumina pipeline version 2.0.2. Average depth of coverage was 45.1×, and 98.3% of the genomes were covered at ≥20×.

VCF (variant call format) files were annotated using ANNOVAR, and the data were filtered on the basis of their predicted effect on protein sequence (nonsense, frameshift, missense, and splice altering), as well as their minor allele frequency (<0.0001) in each of the following publicly available sequencing databases: dbSNP build 129 (www.ncbi.nlm.nih.gov/SNP/), ESP6500 (http://evs.gs.washington.edu/EVS), and 1000 Genomes (http://browser.1000Genomes.org). These databases were last accessed 1 August 2015.

NAF1 sequencing

Genomic DNA was derived from peripheral blood except for a sample that was from archived formalin-fixed paraffin-embedded (FFPE) tissue and another from dried blood spots. To screen for *NAF1* mutations, we used a TruSeq Custom Amplicon panel (Illumina) that included the coding *NAF1* sequence, as well as flanking intronic sequence as described (3). In two cases, we analyzed the *NAF1* sequence from existing exome data that were

generated and analyzed using previously described methods (15). Sanger sequencing was used to confirm variants and test for segregation in family members. The following primers were used for amplification and sequencing of *NAF1* exon 7: 5′-GGCTGATTACTGGCCTGTGTTAA-3′ (forward) and 5′-CCTCCTGCTATGTAATGGCTCTAAA-3′ (reverse) (476 bp). For FFPE tissues, primer sequences were modified to generate a smaller amplicon: 5′-GCATAATAGGCTTATTTTCTTCACC-3′ (forward) and 5′-CAGAGAGAACCCAGATGTTTCCTTC-3′ (reverse) (294 bp).

Mice

Mice were housed in the Johns Hopkins University School of Medicine East Baltimore campus, and all procedures were approved by its Institutional Animal Care and Use Committee. All strains were maintained on the C57BL/6J background. $TR^{+/-}$ and $TR^{-/-}$ mice were generated and maintained as described (37).

Generation of *Naf1*-null mice

Targeting the *Naf1* locus was performed using CRISPR/Cas9 (58). A synthetic single-guide RNA (sgRNA) target sequence (5′-GGTCACCGGCCGGAACGCCG-3′) was designed to target exon 1 of *Naf1* (NC_000074.5) using the Optimized CRISPR Design tool (http://crispr.mit.edu/). This oligonucleotide was cloned into a pX459 plasmid (gift from F. Zhang; Addgene, no. 48139) (59) and appended with a T7 promoter. The sgRNA was in vitro transcribed and purified. The sgRNA and Cas9 (TriLink BioTechnologies) were co-injected into C57BL/6J zygotes (Johns Hopkins Transgenic Core). Pups ($n = 6$) were screened for locus editing by Sanger sequencing: 5′-GCTGCAGACGCTCAAGTTC-3′ (forward) and 5′-AAAGGAAGCGGGAACTCCTA-3′ (reverse) (838-bp wild-type allele). Mice were subsequently genotyped using this primer pair.

TR qRT-PCR

Total RNA was extracted with the RNeasy Mini Kit (Qiagen) as recommended except that deoxyribonuclease digestion was performed using twice the volume and for an extended period of 1 hour. Random hexamer-primed cDNA was synthesized using the SuperScript III Reverse Transcriptase kit (Invitrogen). Quantitative PCR of hTR and mTR was carried out as described (60, 61), respectively. Minor modifications included using freeze-thaw cycles to lyse cell pellets in lysis buffer and homogenization of total mouse spleens using the Bullet Blender (Next Advance). For each experiment, the side-by-side comparisons were made on simultaneously prepared cDNA.

Immunoblotting studies

Immunoblotting was performed as described (60). Briefly, cultured cells were lysed using radioimmunoprecipitation assay buffer supplemented with a protease inhibitor cocktail (Roche). Proteins were resolved with SDS–polyacrylamide gel electrophoresis, and after transfer to a nitrocellulose membrane were blocked in Odyssey blocking buffer (LI-COR). The following primary antibodies were used: human NAF1 (rabbit, ab157106, 1:1000; Abcam), mouse Naf1 (rabbit, Naf1 394, 1:250; Prosci), Myc (mouse, clone 4A6, 1:1000;

Millipore), human dyskerin (rabbit, sc-48794, 1:250; Santa Cruz Biotechnology), and green fluorescent protein (mouse, 7.1 and 13.1, 1:1000; Roche) with loading controls actin (mouse, ab8226, 1:2000; Abcam), tubulin (rabbit, ab6046, 1:5000; Abcam), PARP (rabbit, 9542S, 1:1000; Cell Signaling Technology), or GAPDH (mouse, mAbcam9498, 1:1000; Abcam). Secondary antibodies were conjugated to dyes IR680 or IR800 (donkey, 1:10,000; LI-COR), and blots were visualized using an Odyssey scanner (LI-COR), with exception of the mouse Naf1 antibody that was visualized by horseradish peroxidase–linked antibody (rabbit, 7074, 1:10,000; Cell Signaling Technology) and enhanced chemiluminescent substrate (Thermo Scientific). Cell fractionation was performed using NE-PER Nuclear and Cytoplasmic Extraction Reagents (Thermo Scientific).

Statistical analyses

Statistical comparisons were made with GraphPad Prism software, and all *P* values are two-sided. Student's *t* test was used for comparison of means, and *P* values less than 0.05 were considered significant.

Supplementary Material

Refer to Web version on PubMed Central for supplementary material.

Acknowledgments

We thank the subjects who volunteered for the study, as well as their referring clinicians. We appreciate helpful discussions with A. Holland, J. J.-L. Chen, R. Green, and C. Greider. We are grateful for technical help from C. Connelly, and C. E. Kiefe from the Johns Hopkins Department of Art as Applied to Medicine for help with the figure layouts. We acknowledge support from the Johns Hopkins Genetic Resources Core Facility, the Mouse Phenotyping Core (C. Brayton), Transgenic Core (C. Hawkins), and School of Public Health Flow Cytometry Core (H. Zhang).

Funding: This work was supported by NIH grants CA160433 and HL119476 and the Commonwealth Foundation (to M.A.), K99-R00 HL113105 (to J.K.A.), and the American Cancer Society (ACS)–Robbie Sue Mudd Kidney Cancer Research Scholar grants GM101316 and CA187236 (to W.V.G.). T.M.C. was supported by a fellowship from the ACS New England Division.

REFERENCES AND NOTES

1. Xu J, Murphy SL, Kochanek KD, Bastian BA. Deaths: Final data for 2013. Natl. Vital Stat. Rep. 2016; 64:1–119. [PubMed: 26905861]
2. Stanley SE, Armanios M. The short and long telomere syndromes: Paired paradigms for molecular medicine. Curr. Opin. Genet. Dev. 2015; 33:1–9. [PubMed: 26232116]
3. Stanley SE, Chen JJL, Podlevsky JD, Alder JK, Hansel NN, Mathias RA, Qi X, Rafaels NM, Wise RA, Silverman EK, Barnes KC, Armanios M. Telomerase mutations in smokers with severe emphysema. J. Clin. Invest. 2015; 125:563–570. [PubMed: 25562321]
4. Steele MP, Speer MC, Loyd JE, Brown KK, Herron A, Slifer SH, Burch LH, Wahidi MM, Phillips JA III, Sporn TA, McAdams HP, Schwarz MI, Schwartz DA. Clinical and pathologic features of familial interstitial pneumonia. Am. J. Respir. Crit. Care Med. 2005; 172:1146–1152. [PubMed: 16109978]
5. Silverman EK, Weiss ST, Drazen JM, Chapman HA, Carey V, Campbell EJ, Denish P, Silverman RA, Celedon JC, Reilly JJ, Ginns LC, Speizer FE. Gender-related differences in severe, early-onset chronic obstructive pulmonary disease. Am. J. Respir. Crit. Care Med. 2000; 162:2152–2158. [PubMed: 11112130]

6. Alder JK, Chen JJ-L, Lancaster L, Danoff S, Su S-c, Cogan JD, Vulto I, Xie M, Qi X, Tuder RM, Phillips JA III, Lansdorp PM, Loyd JE, Armanios MY. Short telomeres are a risk factor for idiopathic pulmonary fibrosis. Proc. Natl. Acad. Sci. U.S.A. 2008; 105:13051–13056. [PubMed: 18753630]
7. Armanios M. Telomerase and idiopathic pulmonary fibrosis. Mutat. Res. 2012; 730:52–58. [PubMed: 22079513]
8. Alder JK, Guo N, Kembou F, Parry EM, Anderson CJ, Gorgy AI, Walsh MF, Sussan T, Biswal S, Mitzner W, Tuder RM, Armanios M. Telomere length is a determinant of emphysema susceptibility. Am. J. Respir. Crit. Care Med. 2011; 184:904–912. [PubMed: 21757622]
9. Alder JK, Barkauskas CE, Limjunyawong N, Stanley SE, Kembou F, Tuder RM, Hogan BLM, Mitzner W, Armanios M. Telomere dysfunction causes alveolar stem cell failure. Proc. Natl. Acad. Sci. U.S.A. 2015; 112:5099–5104. [PubMed: 25840590]
10. Tsuji T, Aoshiba K, Nagai A. Alveolar cell senescence in patients with pulmonary emphysema. Am. J. Respir. Crit. Care Med. 2006; 174:886–893. [PubMed: 16888288]
11. Cronkhite JT, Xing C, Raghu G, Chin KM, Torres F, Rosenblatt RL, Garcia CK. Telomere shortening in familial and sporadic pulmonary fibrosis. Am. J. Respir. Crit. Care Med. 2008; 178:729–737. [PubMed: 18635888]
12. Armanios M. Syndromes of telomere shortening. Annu. Rev. Genomics Hum. Genet. 2009; 10:45–61. [PubMed: 19405848]
13. Alder JK, Stanley SE, Wagner CL, Hamilton M, Hanumanthu VS, Armanios M. Exome sequencing identifies mutant *TINF2* in a family with pulmonary fibrosis. Chest. 2015; 147:1361–1368. [PubMed: 25539146]
14. Parry EM, Alder JK, Qi X, Chen JJ-L, Armanios M. Syndrome complex of bone marrow failure and pulmonary fibrosis predicts germline defects in telomerase. Blood. 2011; 117:5607–5611. [PubMed: 21436073]
15. Alder JK, Parry EM, Yegnasubramanian S, Wagner CL, Lieblich LM, Auerbach R, Auerbach AD, Wheelan SJ, Armanios M. Telomere phenotypes in females with heterozygous mutations in the dyskeratosis congenita 1 (*DKC1*) gene. Hum. Mutat. 2013; 34:1481–1485. [PubMed: 23946118]
16. Silhan LL, Shah PD, Chambers DC, Snyder LD, Riise GC, Wagner CL, Hellström-Lindberg E, Orens JB, Mewton JF, Danoff SK, Arcasoy MO, Armanios M. Lung transplantation in telomerase mutation carriers with pulmonary fibrosis. Eur. Respir. J. 2014; 44:178–187. [PubMed: 24833766]
17. Armanios M, Chen J-L, Chang Y-PC, Brodsky RA, Hawkins A, Griffin CA, Eshleman JR, Cohen AR, Chakravarti A, Hamosh A, Greider CW. Haploinsufficiency of telomerase reverse transcriptase leads to anticipation in autosomal dominant dyskeratosis congenita. Proc. Natl. Acad. Sci. U.S.A. 2005; 102:15960–15964. [PubMed: 16247010]
18. Armanios MY, Chen JJ-L, Cogan JD, Alder JK, Ingersoll RG, Markin C, Lawson WE, Xie M, Vulto I, Phillips JA III, Lansdorp PM, Greider CW, Loyd JE. Telomerase mutations in families with idiopathic pulmonary fibrosis. N. Engl. J. Med. 2007; 356:1317–1326. [PubMed: 17392301]
19. Tsakiri KD, Cronkhite JT, Kuan PJ, Xing C, Raghu G, Weissler JC, Rosenblatt RL, Shay JW, Garcia CK. Adult-onset pulmonary fibrosis caused by mutations in telomerase. Proc. Natl. Acad. Sci. U.S.A. 2007; 104:7552–7557. [PubMed: 17460043]
20. Cogan JD, Kropski JA, Zhao M, Mitchell DB, Rives L, Markin C, Garnett ET, Montgomery KH, Mason WR, McKean DF, Powers J, Murphy E, Olson LM, Choi L, Cheng D-S, University of Washington Center for Mendelian Genomics. Blue EM, Young LR, Lancaster LH, Steele MP, Brown KK, Schwarz MI, Fingerlin TE, Schwartz DA, Lawson WE, Loyd JE, Zhao Z, Phillips JA III, Blackwell TS. Rare variants in *RTEL1* are associated with familial interstitial pneumonia. Am. J. Respir. Crit. Care Med. 2015; 191:646–655. [PubMed: 25607374]
21. Stuart BD, Choi J, Zaidi S, Xing C, Holohan B, Chen R, Choi M, Dharwadkar P, Torres F, Girod CE, Weissler J, Fitzgerald J, Kershaw C, Klesney-Tait J, Mageto Y, Shay JW, Ji W, Bilguvar K, Mane S, Lifton RP, Garcia CK. Exome sequencing links mutations in *PARN* and *RTEL1* with familial pulmonary fibrosis and telomere shortening. Nat. Genet. 2015; 47:512–517. [PubMed: 25848748]
22. Mitchell JR, Cheng J, Collins K. A box H/ACA small nucleolar RNA-like domain at the human telomerase RNA 3′ end. Mol. Cell. Biol. 1999; 19:567–576. [PubMed: 9858580]

23. Mitchell JR, Wood E, Collins K. A telomerase component is defective in the human disease dyskeratosis congenita. Nature. 1999; 402:551–555. [PubMed: 10591218]
24. Chen J-L, Blasco MA, Greider CW. Secondary structure of vertebrate telomerase RNA. Cell. 2000; 100:503–514. [PubMed: 10721988]
25. Venteicher AS, Meng Z, Mason PJ, Veenstra TD, Artandi SE. Identification of ATPases pontin and reptin as telomerase components essential for holoenzyme assembly. Cell. 2008; 132:945–957. [PubMed: 18358808]
26. Egan ED, Collins K. Biogenesis of telomerase ribonucleoproteins. RNA. 2012; 18:1747–1759. [PubMed: 22875809]
27. Yu Y-T, Meier UT. RNA-guided isomerization of uridine to pseudouridine—Pseudouridylation. RNA Biol. 2014; 11:1483–1494. [PubMed: 25590339]
28. Schmidt JC, Cech TR. Human telomerase: Biogenesis, trafficking, recruitment, and activation. Genes Dev. 2015; 29:1095–1105. [PubMed: 26063571]
29. Hoareau-Aveilla C, Bonoli M, Caizergues-Ferrer M, Henry Y. hNaf1 is required for accumulation of human box H/ACA snoRNPs, scaRNPs, and telomerase. RNA. 2006; 12:832–840. [PubMed: 16601202]
30. Fatica A, Dlakić M, Tollervey D. Naf1 p is a box H/ACA snoRNP assembly factor. RNA. 2002; 8:1502–1514. [PubMed: 12515383]
31. Darzacq X, Kittur N, Roy S, Shav-Tal Y, Singer RH, Meier UT. Stepwise RNP assembly at the site of H/ACA RNA transcription in human cells. J. Cell Biol. 2006; 173:207–218. [PubMed: 16618814]
32. Goldman F, Bouarich R, Kulkarni S, Freeman S, Du H-Y, Harrington L, Mason PJ, Londoño-Vallejo A, Bessler M. The effect of *TERC* haploinsufficiency on the inheritance of telomere length. Proc. Natl. Acad. Sci. U.S.A. 2005; 102:17119–17124. [PubMed: 16284252]
33. Hao L-Y, Armanios M, Strong MA, Karim B, Feldser DM, Huso D, Greider CW. Short telomeres, even in the presence of telomerase, limit tissue renewal capacity. Cell. 2005; 123:1121–1131. [PubMed: 16360040]
34. Alder JK, Cogan JD, Brown AF, Anderson CJ, Lawson WE, Lansdorp PM, Phillips JA III, Loyd JE, Chen JJ-L, Armanios M. Ancestral mutation in telomerase causes defects in repeat addition processivity and manifests as familial pulmonary fibrosis. PLOS Genet. 2011; 7:e1001352. [PubMed: 21483807]
35. Leulliot N, Godin KS, Hoareau-Aveilla C, Quevillon-Cheruel S, Varani G, Henry Y, Van Tilbeurgh H. The box H/ACA RNP assembly factor Naf1p contains a domain homologous to Gar1p mediating its interaction with Cbf5p. J. Mol. Biol. 2007; 371:1338–1353. [PubMed: 17612558]
36. Kittur N, Darzacq X, Roy S, Singer RH, Meier UT. Dynamic association and localization of human H/ACA RNP proteins. RNA. 2006; 12:2057–2062. [PubMed: 17135485]
37. Blasco MA, Lee H-W, Hande MP, Samper E, Lansdorp PM, DePinho RA, Greider CW. Telomere shortening and tumor formation by mouse cells lacking telomerase RNA. Cell. 1997; 91:25–34. [PubMed: 9335332]
38. Ganot P, Bortolin M-L, Kiss T. Site-specific pseudouridine formation in preribosomal RNA is guided by small nucleolar RNAs. Cell. 1997; 89:799–809. [PubMed: 9182768]
39. Carlile TM, Rojas-Duran MF, Zinshteyn B, Shin H, Bartoli KM, Gilbert WV. Pseudouridine profiling reveals regulated mRNA pseudouridylation in yeast and human cells. Nature. 2014; 515:143–146. [PubMed: 25192136]
40. Terzian T, Box N. Genetics of ribosomal proteins: “Curiouser and curiouser”. PLOS Genet. 2013; 9:e1003300. [PubMed: 23382707]
41. Vulliamy T, Marrone A, Goldman F, Dearlove A, Bessler M, Mason PJ, Dokal I. The RNA component of telomerase is mutated in autosomal dominant dyskeratosis congenita. Nature. 2001; 413:432–435. [PubMed: 11574891]
42. Strong MA, Vidal-Cardenas SL, Karim B, Yu H, Guo N, Greider CW. Phenotypes in $mTERT^{+/-}$ and $mTERT^{-/-}$ mice are due to short telomeres, not telomere-independent functions of telomerase reverse transcriptase. Mol. Cell. Biol. 2011; 31:2369–2379. [PubMed: 21464209]

43. Zhong F, Savage SA, Shkreli M, Giri N, Jessop L, Myers T, Chen R, Alter BP, Artandi SE. Disruption of telomerase trafficking by TCAB1 mutation causes dyskeratosis congenita. Genes Dev. 2011; 25:11–16. [PubMed: 21205863]
44. Walne AJ, Vulliamy T, Marrone A, Beswick R, Kirwan M, Masunari Y, Al-Qurashi F-h, Aljurf M, Dokal I. Genetic heterogeneity in autosomal recessive dyskeratosis congenita with one subtype due to mutations in the telomerase-associated protein NOP10. Hum. Mol. Genet. 2007; 16:1619–1629. [PubMed: 17507419]
45. Vulliamy T, Beswick R, Kirwan M, Marrone A, Digweed M, Walne A, Dokal I. Mutations in the telomerase component NHP2 cause the premature ageing syndrome dyskeratosis congenita. Proc. Natl. Acad. Sci. U.S.A. 2008; 105:8073–8078. [PubMed: 18523010]
46. Codd V, Nelson CP, Albrecht E, Mangino M, Deelen J, Buxton JL, Hottenga JJ, Fischer K, Esko T, Surakka I, Broer L, Nyholt DR, Mateo Leach I, Salo P, Hägg S, Matthews MK, Palmen J, Norata GD, O'Reilly PF, Saleheen D, Amin N, Balmforth AJ, Beekman M, de Boer RA, Böhringer S, Braund PS, Burton PR, de Craen AJ, Denniff M, Dong Y, Douroudis K, Dubinina E, Eriksson JG, Garlaschelli K, Guo D, Hartikainen AL, Henders AK, Houwing-Duistermaat JJ, Kananen L, Karssen LC, Kettunen J, Klopp N, Lagou V, van Leeuwen EM, Madden PA, Mägi R, Magnusson PK, Männistö S, McCarthy MI, Medland SE, Mihailov E, Montgomery GW, Oostra BA, Palotie A, Peters A, Pollard H, Pouta A, Prokopenko I, Ripatti S, Salomaa V, Suchiman HE, Valdes AM, Verweij N, Viñuela A, Wang X, Wichmann HE, Widen E, Willemsen G, Wright MJ, Xia K, Xiao X, van Veldhuisen DJ, Catapano AL, Tobin MD, Hall AS, Blakemore AI, van Gilst WH, Zhu H, CARDIoGRAM Consortium. Erdmann J, Reilly MP, Kathiresan S, Schunkert H, Talmud PJ, Pedersen NL, Perola M, Ouwehand W, Kaprio J, Martin NG, van Duijn CM, Hovatta I, Gieger C, Metspalu A, Boomsma DI, Jarvelin MR, Slagboom PE, Thompson JR, Spector TD, van der Harst P, Samani NJ. Identification of seven loci affecting mean telomere length and their association with disease. Nat. Genet. 2013; 45:422–427e2. [PubMed: 23535734]
47. Pooley KA, Bojesen SE, Weischer M, Nielsen SF, Thompson D, Amin Al Olama A, Michailidou K, Tyrer JP, Benlloch S, Brown J, Audley T, Luben R, Khaw K-T, Neal DE, Hamdy FC, Donovan JL, Kote-Jarai Z, Baynes C, Shah M, Bolla MK, Wang Q, Dennis J, Dicks E, Yang R, Rudolph A, Schildkraut J, Chang-Claude J, Burwinkel B, Chenevix-Trench G, Pharoah PDP, Berchuck A, Eeles RA, Easton DF, Dunning AM, Nordestgaard BG. A genome-wide association scan (GWAS) for mean telomere length within the COGS project: Identified loci show little association with hormone-related cancer risk. Hum. Mol. Genet. 2013; 22:5056–5064. [PubMed: 23900074]
48. Iles MM, Bishop DT, Taylor JC, Hayward NK, Brossard M, Cust AE, Dunning AM, Lee JE, Moses EK, Akslen LA, AMFS Investigators; Andresen PA, Avril M-F, Azizi E, Scarrà GB, Brown KM, Dębniak T, Elder DE, Friedman E, Ghiorzo P, Gillanders EM, Goldstein AM, Gruis NA, Hansson J, Harland M, Helsing P, Hočevar M, Höiom V, IBD Investigators; Ingvar C, Kanetsky PA, Landi MT, Lang J, Lathrop GM, Lubiński J, Mackie RM, Martin NG, Molven A, Montgomery GW, Novaković S, Olsson H, Puig S, Puig-Butille JA, QMEGA and QTWIN Investigators; Radford-Smith GL, Randerson-Moor J, SDH Study Group. van der Stoep N, van Doorn R, Whiteman DC, MacGregor S, Pooley KA, Ward SV, Mann GJ, Amos CI, Pharoah PD, Demenais F, Law MH, Newton Bishop JA, Barrett JH. GenoMEL Consortium. The effect on melanoma risk of genes previously associated with telomere length. J. Natl. Cancer Inst. 2014; 106:dju267. [PubMed: 25231748]
49. Meier UT. The many facets of H/ACA ribonucleoproteins. Chromosoma. 2005; 114:1–14. [PubMed: 15770508]
50. Hathcock KS, Hemann MT, Opperman KK, Strong MA, Greider CW, Hodes RJ. Haploinsufficiency of mTR results in defects in telomere elongation. Proc. Natl. Acad. Sci. U.S.A. 2002; 99:3591–3596. [PubMed: 11904421]
51. Capozzo C, Sartorello F, Dal Pero F, D'Angelo M, Vezzi A, Campanaro S, Valle G. Gene disruption and basic phenotypic analysis of nine novel yeast genes from chromosome XIV. Yeast. 2000; 16:1089–1097. [PubMed: 10953080]
52. Dez C, Noaillac-Depeyre J, Caizergues-Ferrer M, Henry Y. Naf1p, an essential nucleoplasmic factor specifically required for accumulation of box H/ACA small nucleolar RNPs. Mol. Cell. Biol. 2002; 22:7053–7065. [PubMed: 12242285]
53. Cech TR, Steitz JA. The noncoding RNA revolution–trashing old rules to forge new ones. Cell. 2014; 157:77–94. [PubMed: 24679528]

54. Jonassaint NL, Guo N, Califano JA, Montgomery EA, Armanios M. The gastrointestinal manifestations of telomere-mediated disease. Aging Cell. 2013; 12:319–323. [PubMed: 23279657]
55. Gorgy AI, Jonassaint NL, Stanley SE, Koteish A, DeZern AE, Walter JE, Sopha SC, Hamilton JP, Hoover-Fong J, Chen AR, Anders RA, Kamel IR, Armanios M. Hepatopulmonary syndrome is a frequent cause of dyspnea in the short telomere disorders. Chest. 2015; 148:1019–1026. [PubMed: 26158642]
56. Penno MB, Pedrotti-Krueger M, Ray T. Cyropreservation of whole blood and isolated lymphocytes for B-cell immortalization. J. Tissue Cult. Methods. 1993; 15:43–48.
57. Baerlocher GM, Vulto I, de Jong G, Lansdorp PM. Flow cytometry and FISH to measure the average length of telomeres (flow FISH). Nat. Protoc. 2006; 1:2365–2376. [PubMed: 17406480]
58. Wang H, Yang H, Shivalila CS, Dawlaty MM, Cheng AW, Zhang F, Jaenisch R. One-step generation of mice carrying mutations in multiple genes by CRISPR/Cas-mediated genome engineering. Cell. 2013; 153:910–918. [PubMed: 23643243]
59. Ran FA, Hsu PD, Wright J, Agarwala V, Scott DA, Zhang F. Genome engineering using the CRISPR-Cas9 system. Nat. Protoc. 2013; 8:2281–2308. [PubMed: 24157548]
60. Parry EM, Alder JK, Lee SS, Phillips JA III, Loyd JE, Duggal P, Armanios M. Decreased dyskerin levels as a mechanism of telomere shortening in X-linked dyskeratosis congenita. J. Med. Genet. 2011; 48:327–333. [PubMed: 21415081]
61. Vidal-Cardenas SL, Greider CW. Comparing effects of mTR and mTERT deletion on gene expression and DNA damage response: A critical examination of telomere length maintenance-independent roles of telomerase. Nucleic Acids Res. 2010; 38:60–71. [PubMed: 19850716]
62. Avilion AA, Piatyszek MA, Gupta J, Shay JW, Bacchetti S, Greider CW. Human telomerase RNA and telomerase activity in immortal cell lines and tumor tissues. Cancer Res. 1996; 56:645–650. [PubMed: 8564985]
63. Marchler-Bauer A, Derbyshire MK, Gonzales NR, Lu S, Chitsaz F, Geer LY, Geer RC, He J, Gwadz M, Hurwitz DI, Lanczycki CJ, Lu F, Marchler GH, Song JS, Thanki N, Wang Z, Yamashita RA, Zhang D, Zheng C, Bryant SH. CDD: NCBI's conserved domain database. Nucleic Acids Res. 2015; 43:D222–D226. [PubMed: 25414356]
64. Cole C, Barber JD, Barton GJ. The Jpred 3 secondary structure prediction server. Nucleic Acids Res. 2008; 36:W197–W201. [PubMed: 18463136]
65. Lin K, Simossis VA, Taylor WR, Heringa J. A simple and fast secondary structure prediction method using hidden neural networks. Bioinformatics. 2005; 21:152–159. [PubMed: 15377504]
66. Bryson K, McGuffin LJ, Marsden RL, Ward JJ, Sodhi JS, Jones DT. Protein structure prediction servers at University College London. Nucleic Acids Res. 2005; 33:W36–W38. [PubMed: 15980489]
67. Shen B, Zhang J, Wu H, Wang J, Ma K, Li Z, Zhang X, Zhang P, Huang X. Generation of gene-modified mice via Cas9/RNA-mediated gene targeting. Cell Res. 2013; 23:720–723. [PubMed: 23545779]
68. Gassmann R, Holland AJ, Varma D, Wan X, Çivril F, Cleveland DW, Oegema K, Salmon ED, Desai A. Removal of Spindly from microtubule-attached kinetochores controls spindle checkpoint silencing in human cells. Genes Dev. 2010; 24:957–971. [PubMed: 20439434]
69. Lois C, Hong EJ, Pease S, Brown EJ, Baltimore D. Germline transmission and tissue-specific expression of transgenes delivered by lentiviral vectors. Science. 2002; 295:868–872. [PubMed: 11786607]
70. Moyer TC, Clutario KM, Lambrus BG, Daggubati V, Holland AJ. Binding of STIL to Plk4 activates kinase activity to promote centriole assembly. J. Cell Biol. 2015; 209:863–878. [PubMed: 26101219]
71. Lestrade L, Weber MJ. snoRNA-LBME-db, a comprehensive database of human H/ACA and C/D box snoRNAs. Nucleic Acids Res. 2006; 34:D158–D162. [PubMed: 16381836]
72. Sievers F, Wilm A, Dineen D, Gibson TJ, Karplus K, Li W, Lopez R, McWilliam H, Remmert M, Söding J, Thompson JD, Higgins DG. Fast, scalable generation of high-quality protein multiple sequence alignments using Clustal Omega. Mol. Syst. Biol. 2011; 7:539. [PubMed: 21988835]

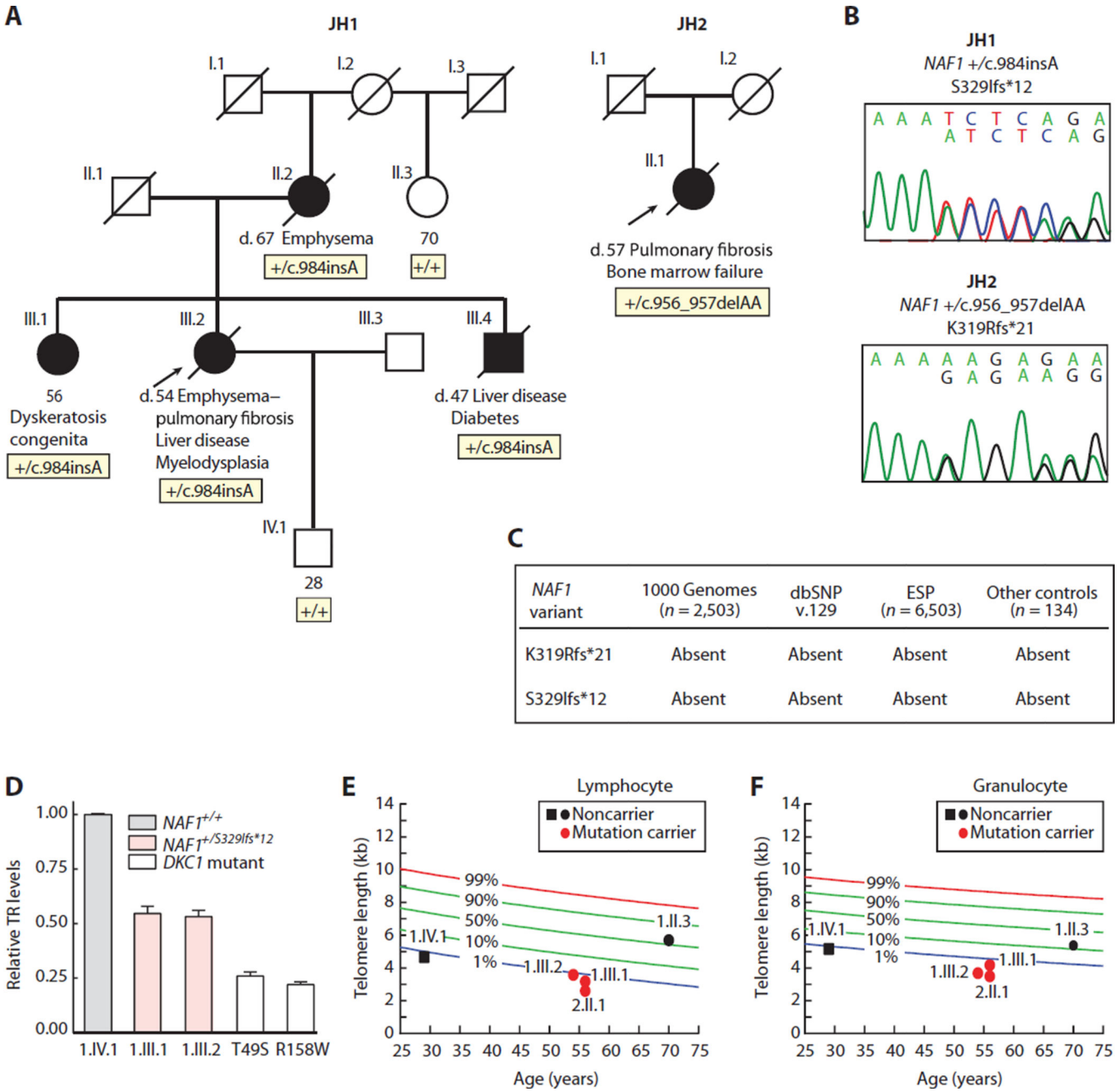

Fig. 1. Rare *NAF1* variants segregate with short telomere disease phenotypes and low TR levels

(**A**) Pedigrees of cases identified in a Johns Hopkins–based Registry (JH1 and JH2) with *NAF1* genotypes shown below the individuals sequenced. NLS, nuclear localization signal. (**B**) Chromatograms of rare *NAF1* variants by Sanger sequencing. (**C**) *NAF1* variants are absent in public databases, as well as additional controls that we sequenced. dbSNP, Single Nucleotide Polymorphism Database; ESP, Exome Sequencing Project. (**D**) TR levels by qRT-PCR in LCLs with pedigree identifiers referring to (A). TR levels from *DKC1* mutation carriers serve as a positive control, and the *DKC1* missense mutations are annotated below. Means are from three separate RNA isolations and experiments, and the error bars represent

SEM. (**E** and **F**) Age-adjusted telomere length in lymphocytes and granulocytes, respectively, measured by flow cytometry and fluorescence in situ hybridization (flow-FISH), with pedigree identifiers corresponding to individuals in (A). The nomogram was constructed from 192 healthy controls, and the calculated percentiles are labeled.

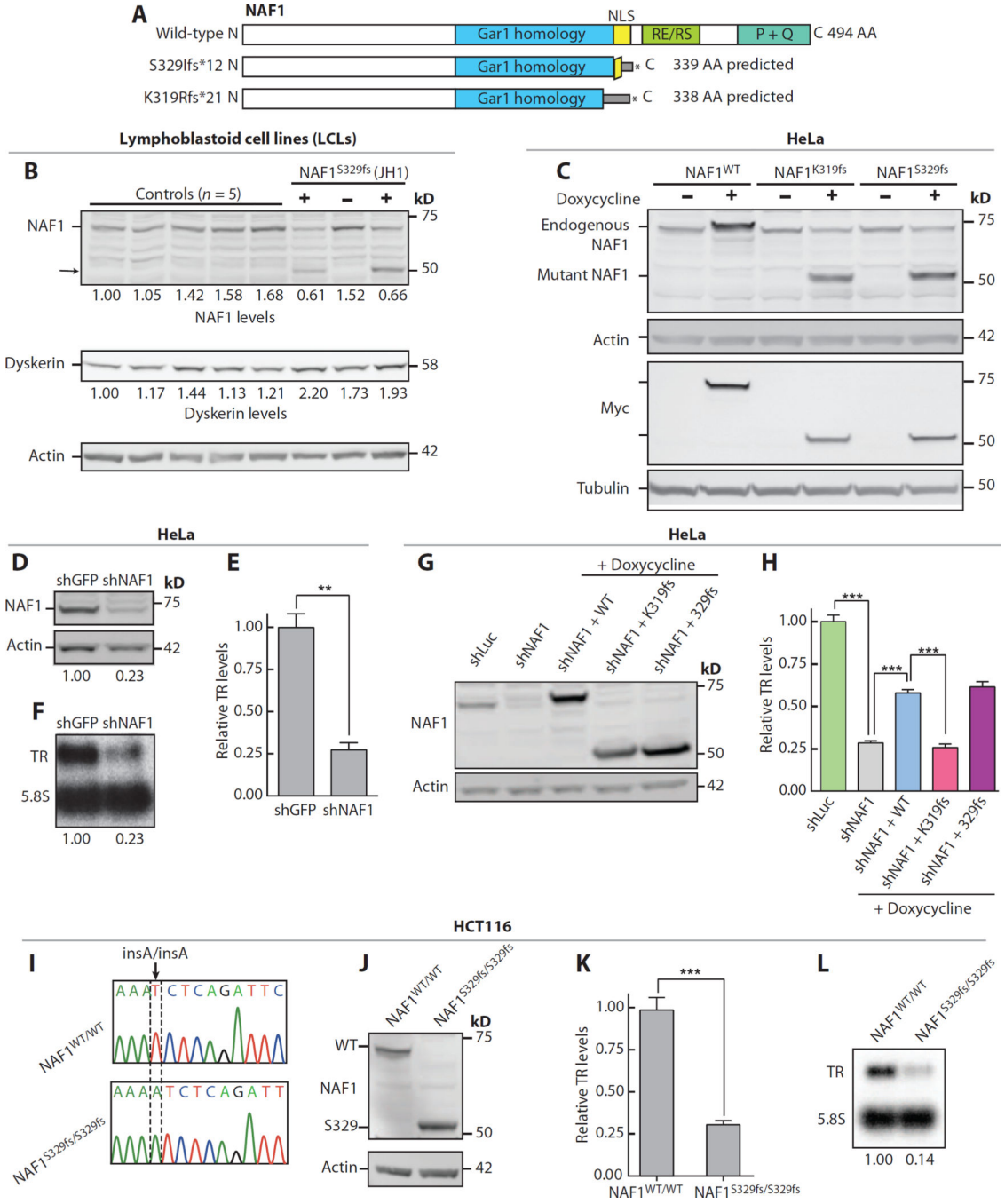

Fig. 2. Disease-associated *NAF1* mutations disturb TR stability

(**A**) Schema of NAF1 protein showing its conserved domains and predicted size of the truncated proteins (NP_612395.2). AA, amino acid. (**B**) Western blot of NAF1 and dyskerin in LCLs derived from unrelated controls and individuals from JH1 family. The "+" refers to NAF1 S329fs heterozygous mutation carriers (1.III.1 and I.III.2), and "−" refers to a noncarrier family member (I.IV.1). Pedigree identifiers refer to Fig. 1A. (**C**)Western blot for Myc-tagged NAF1 at an isogenic doxycycline-inducible locus in HeLa cells. (**D**) Immunoblot of NAF1 in HeLa cells after shRNA knockdown (day 8 time point). (**E** and **F**)

TR levels measured by qRT-PCR and Northern blot, respectively. Mean for qRT-PCR result represents three independent experiments ($P = 0.001$). (**G**) Immunoblot for NAF1 after stable shRNA knockdown in HeLa cells with doxycycline induction of Myc-tagged NAF1. (**H**) TR levels measured by qRT-PCR after stable shRNA knockdown (48 hours after induction). Mean shown is from three technical replicates. *P* value for shLuc versus shNAF is <0.0001, for shNAF1 versus shNAF1 + WT (wild type) is 0.0002, and for shNAF1 + WT versus shNAF1 + K319fs is 0.0003. (**I**) Chromatogram of homozygous c.984insA S329fs disease-associated mutation knocked into the endogenous *NAF1* locus of HCT116 cells using CRISPR/Cas9. (**J**) NAF1 immunoblot on lysates from CRISPR/Cas9-edited HCT116 cells. (**K** and **L**) TR levels quantified by qRT-PCR and Northern blot, respectively. For (K), mean reflects four independent RNA isolations and $P = 0.0001$. Error bars represent SEM. $^{**}P < 0.01$ and $^{***}P < 0.001$ (Student's *t* test).

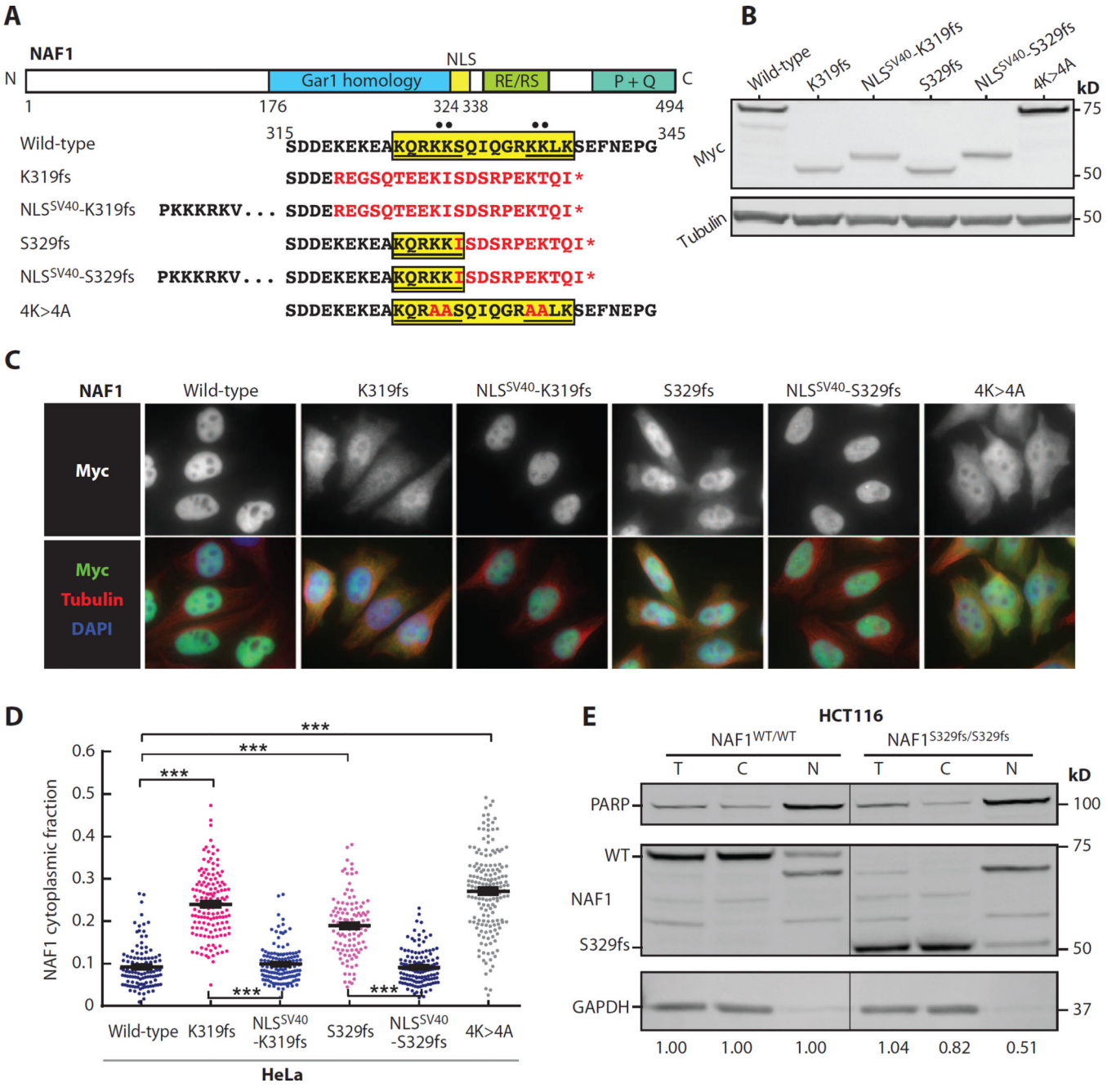

Fig. 3. Mutant NAF1 lacks a C-terminal NLS

(**A**) NAF1 amino acid alignment within and flanking the NLS for disease-associated mutations and those studied for nuclear localization by immunofluorescence are additionally shown. The four conserved lysine residues are indicated by dots above, and the bipartite NLS sequences are underlined. (**B**) Western blot of Myc-tagged NAF1 in the HeLa doxycycline-inducible system after 3-hour exposure to leptomycin B. (**C**) Immunofluorescence images showing subcellular localization of Myc-tagged NAF1 (green). Fluorophores in the three-color overlay are labeled to the left. Images were taken at ×63 magnification (scale bar, 20 μm). DAPI, 4′,6-diamidino-2-phenylindole. (**D**) Quantification

of the NAF1 cytoplasmic fraction represents the intensity of cytoplasmic anti-Myc staining (defined by tubulin-positive area) relative to the nuclear staining (DAPI area). About 100 cells were quantified for each cell line, and mean values are shown with error bars representing SEM. Analysis was performed blinded to genotype. (**E**)Western blot of total (T), cytoplasmic (C), and nuclear (N) protein lysates of parental HCT116 and CRISPR/Cas9-edited HCT116 cells. For the quantification shown below, the total and cytoplasmic fractions were normalized to glyceraldehyde phosphate dehydrogenase (GAPDH), whereas the nuclear fraction was normalized to poly(ADP-ribose) polymerase (PARP). ***$P < 0.001$ (Student's *t* test).

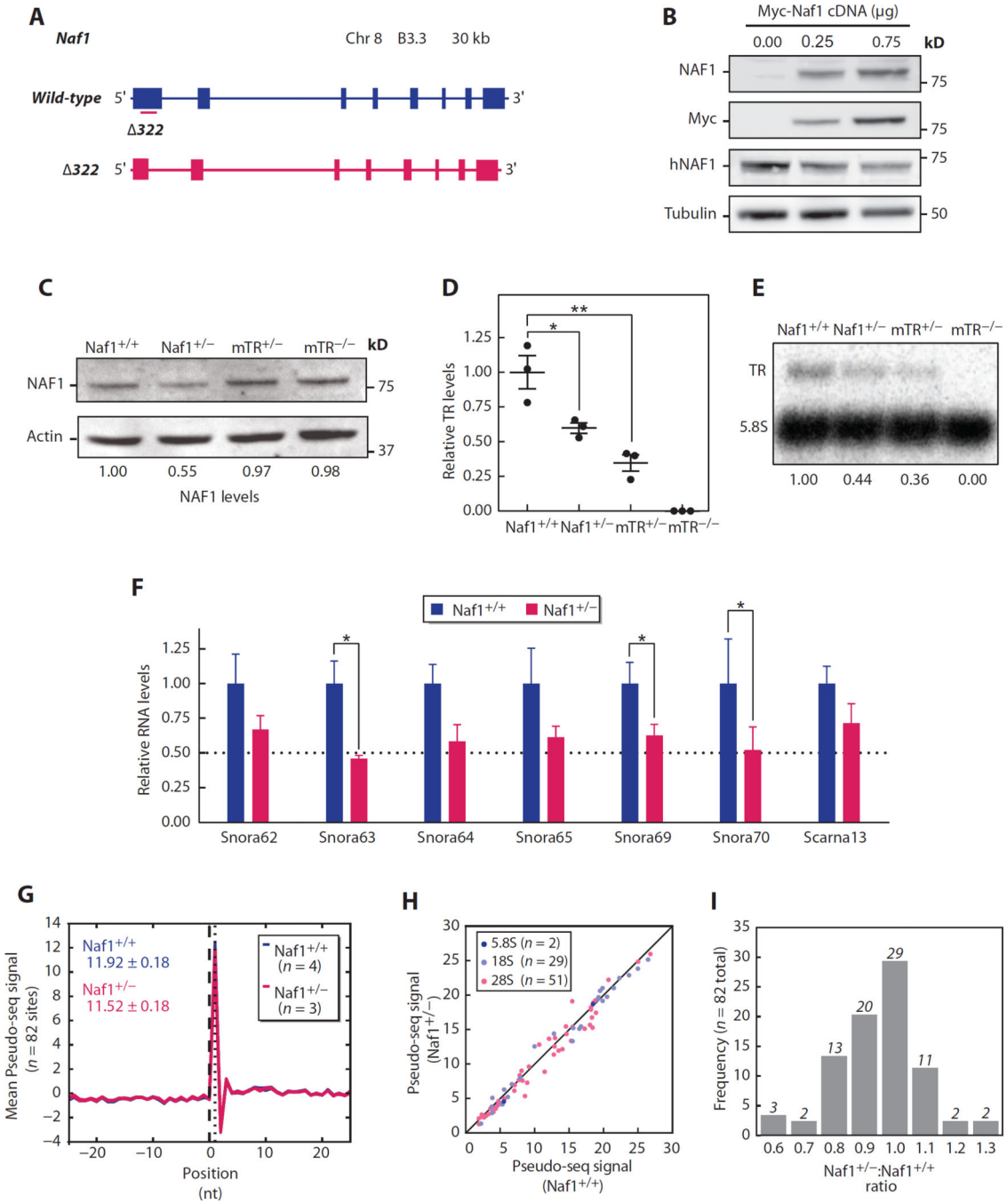

Fig. 4. *Naf1*$^{+/-}$ mice have low TR and snoRNA levels, but rRNA pseudouridylation is intact

(**A**) Schema of *wild-type Naf1* locus and CRISPR/Cas9-induced 322-bp deletion (Δ322) in exon 1. (**B**) Immunoblot of lysate from human embryonic kidney (HEK) 293FT cells transfected with Myc-tagged Naf1 cDNA-containing plasmid at shown concentrations. Immunoblot for human NAF1 (hNAF1) and mouse NAF1 and Myc shows specificity of the murine NAF1 antibody. (**C**) Immunoblot for NAF1 in adult skin fibroblasts. (**D**) TR measured by qRT-PCR (total spleen RNA, $n = 3$ mice per group) and normalized to hypoxanthine-guanine phosphoribosyltransferase (Hprt). For *Naf1*$^{+/+}$ versus *Naf1*$^{+/-}$

comparison, $P = 0.03$; for $Naf1^{+/+}$ versus $mTR^{+/-}$ comparison, $P = 0.008$. (**E**) Northern blot for mTR (mouse TR) normalized to 5.8S. (**F**) H/ACA RNA levels measured by qRT-PCR ($n = 3$ to 8 mice per group, total spleen RNA). P values for the comparisons for Snora63, Snora69, and Snora70 are 0.030, 0.048, and 0.036, respectively. (**G**) Average Pseudo-seq signal for 82 detected rRNA Ψ positions and surrounding 51-nucleotide window are shown in this metaPsi plot derived for $Naf1^{+/+}$ ($n = 4$, blue) and $Naf1^{+/-}$ ($n = 3$, red) mice. The plot includes seven lines in total. Mean values are shown in the left upper corner. (**H**) Scatter plot of average Pseudo-seq signal ratio in $Naf1^{+/+}$ versus $Naf1^{+/-}$ mice graphed for 82 sites in three rRNA subunits. (**I**) Frequency distribution of Pseudo-seq signal ratio in $Naf1^{+/-}$ compared with $Naf1^{+/+}$ mice. Data are expressed as means ± SEM. $*P < 0.05$ and $**P < 0.01$ (Student's t test).